



In situ Raman analyses of deep-sea hydrothermal and cold seep systems (Gorda Ridge and Hydrate Ridge)

S. N. White

Monterey Bay Aquarium Research Institute, 7700 Sandholdt Road, Moss Landing, California 95039, USA

*Now at Woods Hole Oceanographic Institution, Blake 209, MS#7, Woods Hole, Massachusetts 02543, USA
(swhite@whoi.edu)*

R. M. Dunk and E. T. Peltzer

Monterey Bay Aquarium Research Institute, 7700 Sandholdt Road, Moss Landing, California 95039, USA

J. J. Freeman

Department of Earth and Planetary Sciences, Washington University, St. Louis, Missouri 63130-4899, USA

P. G. Brewer

Monterey Bay Aquarium Research Institute, 7700 Sandholdt Road, Moss Landing, California 95039, USA

[1] The Deep Ocean Raman In Situ Spectrometer (DORISS) instrument was deployed at the Sea Cliff Hydrothermal Field and Hydrate Ridge in July 2004. The first in situ Raman spectra of hydrothermal minerals, fluids, and bacterial mats were obtained. These spectra were analyzed and compared to laboratory Raman measurements of standards and samples collected from the site. Spectra of vent fluid ($\sim 294^\circ\text{C}$ at the orifice) at ~ 2700 m depth were collected with noncontact and immersion sampling optics. Compared to spectra of ambient ($\sim 2^\circ\text{C}$) seawater, the vent fluid spectra show changes in the intensity and positions of the water O-H stretch bands due to the elevated temperature. The sulfate band observed in seawater spectra is reduced in vent fluid spectra as sulfate is removed from vent fluid in the seafloor. Additional components of hydrothermal fluid are present in concentrations too low to be detected with the current Raman system. A precision underwater positioner (PUP) was used to focus the laser spot on opaque samples such as minerals and bacterial mats. Spectra were obtained of anhydrite from actively venting chimneys, and of barite deposits in hydrothermal crusts. Laboratory analysis of rock samples collected in the vent field also detected the presence of gypsum. Spectra of bacterial mats revealed the presence of elemental sulfur (S_8) and the carotenoid beta-carotene. Challenges encountered include strong fluorescence from minerals and organics and insufficient sensitivity of the instrument. The next generation DORISS instrument addresses some of these challenges and holds great potential for use in deep-sea vent environments.

Components: 7346 words, 12 figures, 1 table.

Keywords: cold seeps; hydrothermal vents; Raman spectroscopy.

Index Terms: 4832 Oceanography: Biological and Chemical: Hydrothermal systems (0450, 1034, 3017, 3616, 8135, 8424); 4894 Oceanography: Biological and Chemical: Instruments, sensors, and techniques; 4825 Oceanography: Biological and Chemical: Geochemistry.

Received 29 November 2005; **Revised** 17 March 2006; **Accepted** 30 March 2006; **Published** 25 May 2006.

White, S. N., R. M. Dunk, E. T. Peltzer, J. J. Freeman, and P. G. Brewer (2006), In situ Raman analyses of deep-sea hydrothermal and cold seep systems (Gorda Ridge and Hydrate Ridge), *Geochem. Geophys. Geosyst.*, 7, Q05023, doi:10.1029/2005GC001204.



1. Introduction

[2] Laser Raman spectroscopy is a noninvasive, nondestructive form of vibrational spectroscopy that is capable of in situ geochemical analyses of gases, liquids and solids in extreme environments. Thus it has great potential for use in deep sea hydrothermal vent environments where targets of interest such as high-temperature vent fluids, fragile chimney structures and bacterial mats may be either too hot for contact analysis or altered when brought to the surface for ship- or shore-based analysis. Raman spectroscopy has been widely used in laboratory settings to analyze simulations of hydrothermal vent fluids [Battaglia *et al.*, 2004; Brill, 2000; Frantz, 1998, 2000; Schoppelrei *et al.*, 1996], targets commonly associated with vents such as precipitates [e.g., Rochette *et al.*, 2000] and bacterial mats [Pasteris *et al.*, 2001], and microbial weathering of sulfide minerals [McGuire *et al.*, 2001], but has not yet been used on such targets in situ.

[3] There are some challenges to using Raman spectroscopy as an in situ technique. Until very recently, Raman systems have been so bulky and fragile that development of an in situ system could not be reasonably considered. The Raman effect is weak (only 1 in 10^8 photons is Raman scattered) so that trace species can be difficult to detect. With the small focal-volume optics used, precise positioning of the laser spot is necessary for acquisition of Raman spectra from solid, opaque targets. Precision positioning cannot yet be achieved by robotic manipulators generally employed on remotely operated vehicles (ROVs).

[4] Many of these problems have recently been overcome with the development of the first generation of ocean laser Raman systems [Brewer *et al.*, 2004a; Pasteris *et al.*, 2004], that have now been applied to the study of gas fractionation rates in the deep-sea [White *et al.*, 2006], and to the in situ measurement of the crystal structure and composition of clathrate hydrates [Hester *et al.*, 2006]. The extension to seafloor measurement of opaque minerals is made possible by coupling the Raman system with a precise beam positioner (Precision Underwater Positioner (PUP)) [White *et al.*, 2005] so that focusing and scanning of the laser beam across a solid surface in the deep sea can yield information on the mineral composition. Such a technique has been widely discussed for planetary exploration and prototype systems have been built [Haskin *et al.*, 1997; Wang *et al.*, 1998, 2003].

[5] In this paper we describe the deployment of DORISS/PUP in the Sea Cliff Hydrothermal Field on Gorda Ridge. Four dives were made at the site using the ROV *Tiburón*. During these dives we attempted to collect spectra from high temperature vent fluid, chimney minerals, hydrothermal crusts, and bacterial mats. Additional bacterial mat spectra were collected at Hydrate Ridge on subsequent dives. The data collected on these dives demonstrate the usefulness of laser Raman spectroscopy as an in situ technique for geochemical measurements in the deep ocean, provide a direct link between laboratory simulations and real vent systems [Brill, 2000; Frantz *et al.*, 1993; Schoppelrei *et al.*, 1996], and provide guidance for future development.

2. Geological Settings

2.1. Sea Cliff Hydrothermal Field

[6] The Sea Cliff Hydrothermal Field (formerly called GR-14) is located on the northern segment of the Gorda Ridge approximately 200 km off the coast of Oregon. Northern Gorda Ridge is an intermediate-spreading rate segment (~ 55 mm/yr [Riddihough, 1980]), and exhibits an axial high with a well defined rift valley [Rona and Clague, 1989]. Sea Cliff Hydrothermal Field is located ~ 2.6 km east of the neovolcanic zone on the rift valley wall ($42^{\circ}45.35'N$, $126.^{\circ}42.52'W$) at a depth of 2675–2800 m (300 m above the valley floor). This site was first identified by water column anomalies in 1986 [Baker *et al.*, 1987], and first visited by the U. S. Navy submersible DSV *Sea Cliff* in 1988 [Rona *et al.*, 1990].

[7] Active venting is concentrated along two ridges which trend perpendicular to the slope of the eastern axial valley wall (022°). The chimneys formed along these ridges are primarily composed of anhydrite and smectite with minor sulfide phases. The seafloor in the area is covered with a hydrothermal crust which consists of altered basalt, barite, amorphous silica, and sulfides (J. S. McClain *et al.*, Observations of the Sea Cliff (GR-14) Hydrothermal Field on the Gorda Ridge: Controls on field geometry and temporal changes, submitted manuscript, 2006). Large areas of the vent field between the ridges are covered with mats of blue organisms believed to be a type of ciliate. White bacterial mat material was also observed on active chimneys.

[8] The hydrothermal vent fluids are essentially clear with exit temperatures as high as $300^{\circ}C$.



Fluid samples collected in 2000, 2002 and 2004 revealed low salinity, vapor phase fluids (17% depletion in Cl relative to seawater) with low metal contents and low pH (~ 4.5 at 25°C) [Von Damm *et al.*, 2006]. Dissolved gas concentrations have been measured to be: $\text{CO}_2 \sim 16$ mmol/kg, $\text{CH}_4 \sim 0.05$ mmol/kg, $\text{H}_2 \sim 0.06$ mmol/kg, $\text{H}_2\text{S} \sim 2.4$ mmol/kg [Von Damm *et al.*, 2006].

2.2. Hydrate Ridge

[9] Hydrate Ridge is a $25 \text{ km} \times 15 \text{ km}$ ridge located on the Cascadia Margin ~ 90 km west of Newport, Oregon. It consists of two summits: North Hydrate Ridge (NHR) at ~ 600 m depth ($44^\circ 40' \text{N}$, $125^\circ 06' \text{W}$), and South Hydrate Ridge (SHR) at ~ 800 m depth ($44^\circ 34' \text{N}$, $125^\circ 09' \text{W}$). The Hydrate Ridge site was drilled by the Ocean Drilling Program in 1992 (Leg 146) and 2002 (leg 204). Active natural gas vents and near-surface seafloor clathrate hydrates are present on both summits [Suess *et al.*, 1999; Torres *et al.*, 2002; Tryon *et al.*, 2002]. Carbonate crusts are also present and consist of high-magnesium calcite and aragonite [Bohrmann *et al.*, 1998; Suess *et al.*, 1999]. Bacterial (*Beggiatoa*) mats, clam (*Calyptogena*) fields, and clam debris have been observed on the summits of both NHR and SHR [Boetius *et al.*, 2000; Torres *et al.*, 2002].

3. Instrumentation and Methods

3.1. Deep Ocean Laser Raman Spectrometer

[10] In situ measurements were made with the DORISS (Deep Ocean Raman In Situ Spectrometer) instrument [Brewer *et al.*, 2004a; Pasteris *et al.*, 2004] deployed by the ROV *Tiburon*. DORISS is a laboratory model laser Raman spectrometer from Kaiser Optical Systems, Inc. (KOSI) that has been modified for use in the deep ocean. The instrument consists of a 532 nm (green) Nd:YAG laser, a holographically filtered probe head with interchangeable optics, a HoloPlex[™] duplex holographic grating, and a 512×2048 pixel CCD camera from Andor Technology. The duplex grating splits the $100\text{--}4400 \text{ cm}^{-1}$ spectral region into two stripes on the face of the CCD, providing a mapping of $\sim 1 \text{ cm}^{-1}/\text{pixel}$. The instrument resolution (determined from the full width at half maximum of narrow bands in the neon emission spectrum) was approximately 4 cm^{-1} . Two types of sampling optics were used on this deployment. A noncontact optic housed behind a domed pres-

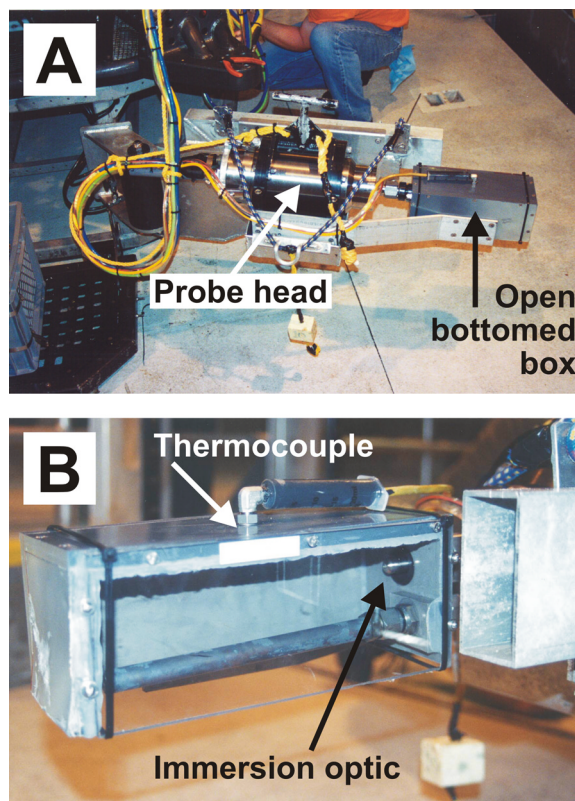


Figure 1. (a) The DORISS optical head with (b) an immersion sampling optic protruding into an open-bottomed box. The optical head is lifted by a T-handle using the ROV manipulator and placed over the vent orifice. A thermocouple inserted into the top of the box provides temperature readings. This configuration is also used to sample natural gas venting from the seafloor, and the long tube in the bottom half of the box is a heater used to melt hydrate formed while collecting gas in the hydrate stability zone.

sure window was used when analyzing opaque targets (i.e., rocks, bacterial mats) and vent fluid exiting the chimney orifice. The working distance of the noncontact optic is ~ 15 cm. A motorized stage inside the pressure housing provides a means of fine-focusing the position of the laser spot when using this optic in a horizontal orientation. An immersion optic with an ~ 2 mm working distance was used in an open bottomed sampling box to analyze buoyant hydrothermal fluid collected above the vent orifice (Figure 1).

[11] The Raman instrument was calibrated the night before each dive using a neon source for the wavelength calibration and a calibrated tungsten light source for intensity calibration. A diamond chip in the laser path inside the probe head provides a reference Raman shift calibration line

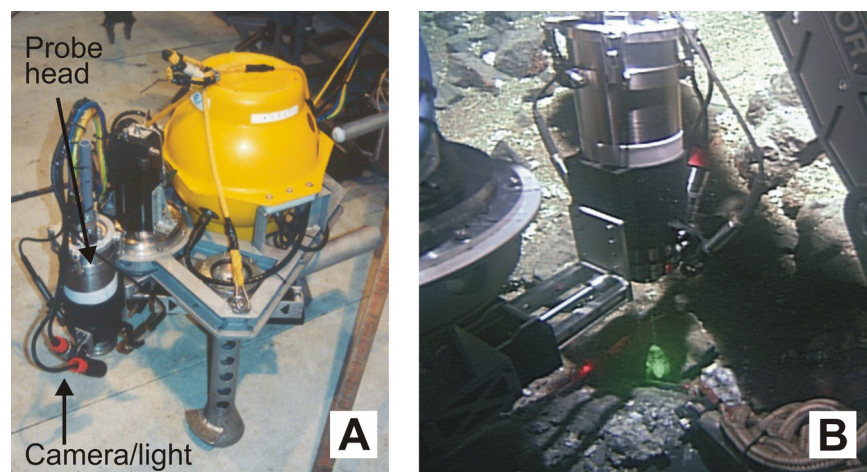


Figure 2. The Precision Underwater Positioner (PUP) is used to position the DORISS optical head at opaque targets on the seafloor. (a) The PUP is a tripod with three degrees of motion. A camera/light and crossing HeNe lasers are used to aid in positioning the laser spot. (b) PUP, mounted on the ROV swing arm, is used to position the optical head over a rock on the seafloor just past the ROV porch. Part of the ROV manipulator is on the right, and PUP's rotational bearing is on the left.

(1332 Δcm^{-1}) that is superimposed on all of the spectra [Brewer *et al.*, 2004a].

[12] Due to stringent positioning requirements when focusing the laser on opaque objects, a precision underwater positioner (PUP) was used to position the DORISS optical head at solid, opaque targets (Figure 2). PUP is a three-degree of freedom positioner that is capable of moving a sensor head in 0.1 mm increments [White *et al.*, 2005]. A camera, light, and crossing HeNe lasers assist the user in focusing the DORISS laser on the target surface. PUP was mounted to a swing-arm on the ROV during the deployment. In this configuration, PUP could position the optical head at a target on the seafloor in front of the ROV or on a collected sample placed on the ROV porch.

[13] Spectra were acquired using KOSI's HoloGRAMS software. Each collected spectrum was an average of nominally 10 accumulations with exposure times of 10–30 seconds (depending on the scattering strength of the target). The ROV's external lights, which produce a number of peaks across the spectral region, were turned off or away during acquisition. Dark subtraction and wavelength and intensity correction were performed by HoloGRAMS during acquisition and the processed spectra were saved in GRAMS/AI software spectrum (.spc) format.

3.2. Laboratory Raman Analyses

[14] Laboratory Raman analyses were conducted on mineral samples collected from the Sea Cliff

Hydrothermal Field. The KOSI laboratory instrument consists of an Invictus 532 nm Nd:YAG laser, a NRxn Spectrograph with a HoloPlex[™] duplex holographic grating, and a 1024 × 127 pixel CCD camera from Andor Technology. The duplex grating splits the 100–4400 Δcm^{-1} spectral region into two stripes on the face of the CCD, providing a mapping of $\sim 2 \text{ cm}^{-1}/\text{pixel}$. The holographically filtered probe head was fitted to a Leica DM LP microscope with a 10X objective ($\sim 19 \text{ mW}$ of laser power). The instrument resolution was $\sim 7 \text{ cm}^{-1}$. Calibration was performed using a neon source for the wavelength calibration, and a tungsten source for intensity calibration.

3.3. Sampling of Vent Fluids

[15] Two configurations were used to collect in situ Raman spectra from high-temperature hydrothermal vent fluids (Figure 3). On *Tiburón* dive 695, a noncontact optic (laser power $\sim 35 \text{ mW}$) was used behind a domed pressure window. The laser spot was focused within a plume of hydrothermal fluid just above the chimney orifice. This optic has a 15 cm working distance and a $\sim 3 \text{ mm}$ depth of focus. Ambient seawater, present in the unfocused portion of the optical path will produce a small water signal in the acquired spectra. On *Tiburón* dive 696, an immersion optic (laser power $\sim 29 \text{ mW}$) was used protruding into an open-bottomed sampling box (Figure 1). The sampling box was held over the vent orifice to collect the buoyant vent fluid. A temperature sensor in the top of the box was used to monitor the fluid temper-

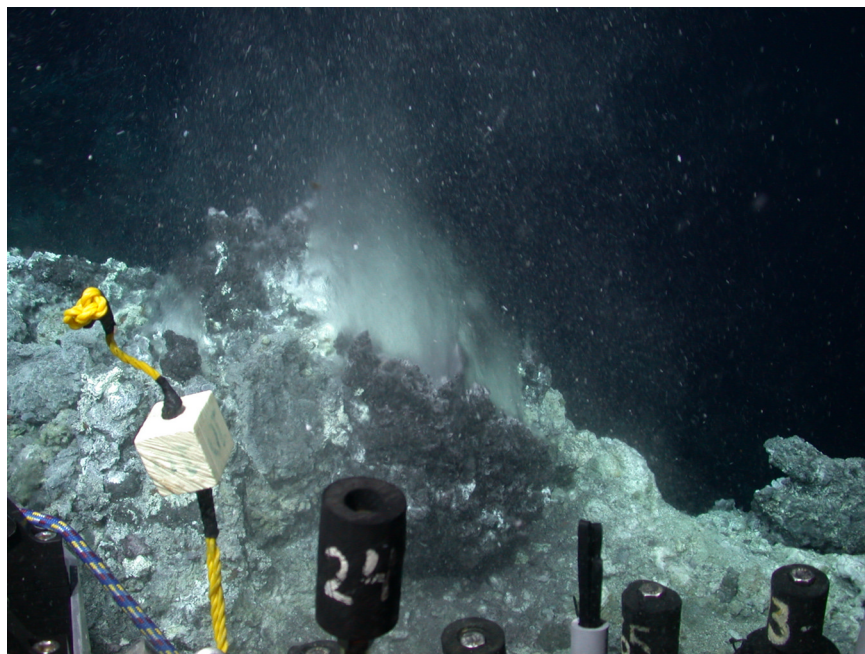


Figure 3. High-temperature ($\sim 294^{\circ}\text{C}$) vent in the Sea Cliff Hydrothermal Field. The exiting fluids are fairly clear. Push core handles mounted on the ROV are in the foreground.

ature. Using this type of configuration, the optic is immersed in a mixture of vent fluid and entrained ambient seawater, and the optical path is essentially uniform in temperature and composition.

[16] Vent fluid temperature measurements and water samples were also collected during these dives. On *Tiburón* dive 695, vent fluid was collected in two major-pair titanium water samplers from a 294°C vent at Marker T (2727 m depth). The water samples were sent to K. Von Damm for analysis [Von Damm *et al.*, 2006]. In situ Raman spectra were collected with the noncontact optic at this vent (Marker T), and at a second vent at a depth of 2720 m, which had an internal orifice temperature of 254°C . The temperature of the fluid as it exited the orifice was measured to be $\sim 157^{\circ}\text{C}$. On *Tiburón* dive 696, in situ Raman spectra were collected with the immersion optic of a 299°C vent located at a depth of 2706 m. We deployed a pink flamingo marker (“Pinkie”) near this vent.

3.4. Data Processing

[17] Postdive spectral analysis was performed using GRAMS/AI data processing software (Thermo Electron Corporation). The Raman shifted peak position, peak height and area were determined using the GRAMS/AI peak fitting routine. This routine calculates and subtracts the baseline, and then uses an iterative technique to fit mixed

Gaussian-Lorentzian peaks to the data and minimize the χ^2 value. When analyzing the same set of peaks in different spectra, the same wave number region was used in the peak fitting routine.

4. Data and Analysis

4.1. Raman Spectra of Vent Fluids

[18] An in situ Raman spectrum of ambient seawater (2°C , 2727 m depth) acquired at the Sea Cliff site is shown in Figure 4. The characteristic seawater peaks are due to the bending mode ($\nu_2 \sim 1640 \Delta\text{cm}^{-1}$) and a set of vibrational modes of the water molecule (3000–3800 Δcm^{-1} region), and the symmetric stretch of the sulfate ion ($\text{SO}_4^{2-} \sim 981 \Delta\text{cm}^{-1}$). The water vibrations in the 3000 to 3800 Δcm^{-1} region consists of a complex profile of several broad and overlapping bands, and the interpretation of this region remains controversial. One explanation is that the high frequency peaks are assigned to the symmetric (ν_1) and antisymmetric (ν_3) OH stretch and the lower-frequency band is due to Fermi resonance with the bending vibration overtone ($2\nu_2$) [Busing and Hornig, 1961; Walrafen, 1964]. However, this later effect has been shown to be either weak or absent [e.g., Terpstra *et al.*, 1990]. An alternative interpretation assigns the bands to a particular configuration of hydrogen-bonded molecules, shifting from domi-

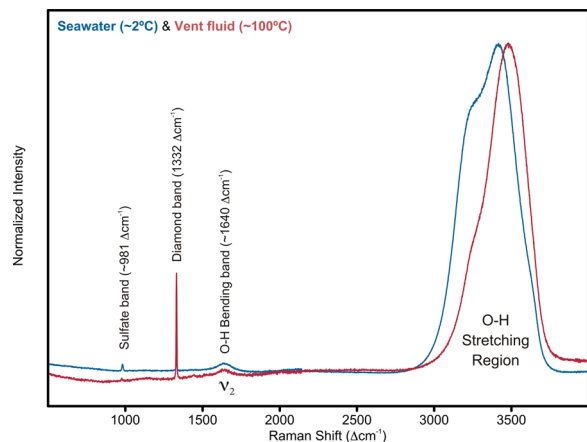


Figure 4. Raman spectra of ambient seawater ($\sim 2^{\circ}\text{C}$, 2727 m depth) and hydrothermal vent fluid ($\sim 100^{\circ}\text{C}$, 2706 m depth). The spectra have been intensity normalized. The vent fluid spectrum was obtained using the immersion optic; therefore no ambient seawater is in the optical path. At higher temperatures the O-H stretching bands of water are shifted to higher wave numbers, and the intensities change. Sulfate is removed from vent fluid in the subseafloor. The small sulfate band observed in the vent fluid spectrum is due to mixing with ambient seawater after exiting the orifice. The diamond band ($1332\ \Delta\text{cm}^{-1}$) provides a calibration reference.

nantly hydrogen bonded molecules in the low frequency region to dominantly nonhydrogen bonded molecules in the high frequency region [e.g., Abe and Ito, 1978].

[19] Data in the literature show that the water bands in the $3000\text{--}3800\ \Delta\text{cm}^{-1}$ region are affected by temperature, pressure, and salinity [e.g., Becucci

et al., 1999; Kawamoto et al., 2004; Ratcliffe and Irish, 1982]. Increasing pressure (on the order of GPa) tends to shift the band positions to lower wave numbers. However, at deep ocean pressures (on the order of MPa), the effect is very slight, on the order of a few wave numbers at most (Table 1). The spectra acquired from Sea Cliff were collected at pressures of $\sim 26.8\text{--}28.0$ MPa. Temperature, and to a lesser extent salinity, has a far greater effect on band positions. The data show that increasing water temperature causes a shift of the OH-stretching bands positions to higher wave numbers and a change in band intensity.

[20] Vent fluid is seawater that has been altered by interaction with hot magma and the crust deep below the seafloor. It is enriched in metals and gases, and depleted in sulfate. Thus the Raman spectrum of vent fluid should contain bands from high temperature water, a reduced sulfate band, and bands from Raman-active constituents such as H_2S , CH_4 and CO_2 . Raman spectra of vent fluid collected with both the noncontact optic and the immersion optic do indicate high-temperature water with little to no sulfate. Raman spectra of ambient seawater and hydrothermal fluid are compared in Figure 4. By performing a simple three band deconvolution of the OH-stretching region, the two temperature effects discussed above can be observed (Figure 5). Band position shifts on the order of 30–40 wave numbers are observed, and the ratio of the intensities of the first two bands also changes significantly as the water temperature increases (Table 1, Figure 5).

[21] In the vent fluid spectra, a decrease in the sulfate band was observed (Figure 4). This is

Table 1. Raman Shift, Peak Widths, and Normalized Peak Intensity of OH-Stretch Water Bands at Ocean Temperatures and Pressures

File Name	Pressure, MPa	Temp., $^{\circ}\text{C}$	OH-Stretch Raman Bands								
			Raman Shift	Peak Width	Normalized Intensity ^a	Raman Shift	Peak Width	Normalized Intensity ^a	Raman Shift	Peak Width	Normalized Intensity ^a
<i>Ambient Seawater</i>											
07180001	7.01	4	3219	226	0.77	3436	250	1.0	3624	101	0.05
07180002	7.51	4	3218	225	0.76	3435	251	1.0	3624	100	0.05
07170018	14.92	2.6	3217	226	0.77	3434	251	1.0	3623	102	0.05
07170017	16.61	2.5	3216	225	0.76	3434	251	1.0	3622	96	0.04
07170004	27.28	1.8	3213	224	0.72	3432	259	1.0	3624	83	0.05
<i>Vent Fluid</i>											
07180005	27.16	100	3248	253	0.33	3475	253	1.0	3598	129	0.10
07180006	27.07	100	3249	210	0.31	3477	252	1.0	3596	129	0.06
07180007	27.07	100	3251	214	0.31	3479	250	1.0	3596	128	0.07

^aNormalized intensity is the peak area of the band normalized to the peak area of the center OH-stretch band.

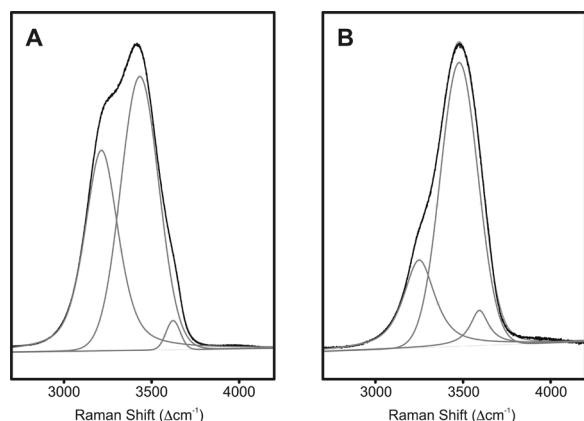


Figure 5. The O-H stretching region of the Raman spectra from (a) ambient ($\sim 2^\circ\text{C}$) seawater at 2627 m depth and (b) hydrothermal vent fluid ($\sim 100^\circ\text{C}$) at 2706 m depth. The signal is deconvolved into three bands. The positions of the bands and their intensities relative to one another are affected by changes in temperature, pressure, and salinity.

expected because vent fluid is depleted of sulfate in the sub-seafloor. Raman bands due to other potential constituents noted above were not observed. On the basis of previous sampling at this site, gas concentrations are expected to be $\text{CO}_2 \sim 16$ mmol/kg, $\text{CH}_4 \sim 0.05$ mmol/kg, $\text{H}_2 \sim 0.06$ mmol/kg, $\text{H}_2\text{S} \sim 2.4$ mmol/kg [Von Damm *et al.*, 2006]. The inability to observe these components is most likely due to a combination of factors such as the instrument sensitivity and the optical characteristics of the plume. Although the fluid exiting the orifice is relatively clear, its turbulence appeared to prevent the focusing of the laser due to the rapidly changing index of refraction which disrupts the optical path. Additionally, when using the immersion optic, contact with the vent fluid led to the build-up of a sulfide particle coating on the sapphire window that reduced the optical throughput over time.

4.2. Raman Spectra of Minerals

[22] Raman spectra were collected of chimney material and hydrothermal crusts in the Sea Cliff Hydrothermal Field. PUP was used to position the DORISS optical head over rocks on the seafloor and chimney samples broken off and placed on the ROV porch for analysis (Figure 2). Two minerals were primarily observed with the DORISS instrument. Barite (BaSO_4) was detected as thin rinds or veins in the hydrothermal crust found between the ridges of active chimneys (Figure 6). Barite is identified by a primary band at ~ 987 Δcm^{-1} and a secondary band at ~ 457 Δcm^{-1} . In some cases

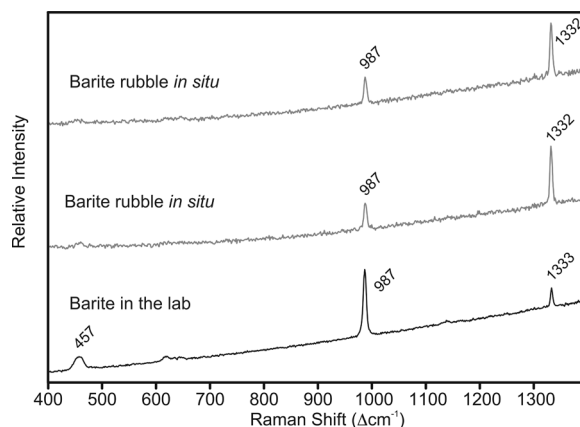


Figure 6. Raman spectra of barite obtained in situ in the Sea Cliff Field and in the lab. In the two seafloor spectra, the 987 Δcm^{-1} barite band is strong enough to completely obscure the 981 Δcm^{-1} sulfate band in seawater (seawater is in the optical path).

the 987 Δcm^{-1} band was strong enough to completely obscure the 981 Δcm^{-1} sulfate band, while in other spectra, a broadened band was observed which could be deconvolved into the 981 and 987 Δcm^{-1} bands. The darker material surrounding the barite veins was found to have significant fluorescence. The sample with barite veins analyzed in situ was recovered and analyzed in the lab with the Raman microprobe. The laboratory results matched the in situ results with only barite detected.

[23] The active chimneys at Sea Cliff are primarily anhydrite (CaSO_4). Anhydrite is generally the first

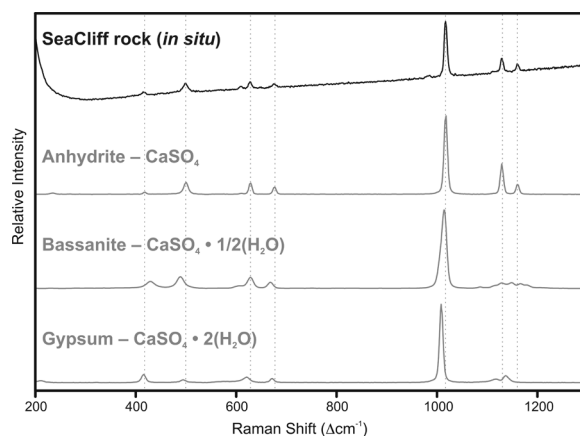


Figure 7. Raman spectrum of a Sea Cliff rock compared to spectra of three species of calcium sulfate: anhydrite (CaSO_4), gypsum ($\text{CaSO}_4 \bullet 2(\text{H}_2\text{O})$), and bassanite ($\text{CaSO}_4 \bullet 1/2(\text{H}_2\text{O})$). The primary bands observed in the in situ spectrum correspond well to anhydrite (dashed lines).



mineral phase precipitated at a high-temperature vent [Tivey, 1995], as the Ca-enriched, SO_4 -depleted vent fluid mixes with SO_4 -rich ambient seawater. Anhydrite has retrograde solubility, and will dissolve at temperatures below 130°C [Haymon and Kastner, 1981], and thus is not observed away from high-temperature venting. In the case of black smoker vents, anhydrite in the chimney walls is replaced by sulfide minerals such as chalcopyrite. Anhydrite in collapsed chimneys is replaced by the more stable gypsum ($\text{CaSO}_4 \bullet 2(\text{H}_2\text{O})$) at ambient seawater temperatures. Gypsum replacement has been observed in collapsed chimneys in the Sea Cliff site [Von Damm et al., 2006].

[24] Anhydrite (CaSO_4), gypsum ($\text{CaSO}_4 \bullet 2(\text{H}_2\text{O})$) and bassanite ($\text{CaSO}_4 \bullet 1/2(\text{H}_2\text{O})$) are all common calcium sulfate minerals. These three calcium sulfate species can be distinguished from one another by their Raman spectra. The in situ spectra collected from chimney material at Sea Cliff clearly show the presence of anhydrite (Figure 7). Samples of active and collapsed chimneys were collected and analyzed postcruise with a laboratory Raman microprobe. Data collected in the lab was similar to data collected in situ. Chimney samples, both active and collapsed showed the presence of anhydrite. Green coatings on these pieces exhibited strong fluorescence with no discernable peaks.

[25] A slab of hydrothermal crust was collected on Tiburon dive 696 at the base of the vent field. This sample was not analyzed in situ. The surface of the slab was dark brown to black, with areas of green coating and rust staining. The interior was white and fine-grained. Strong fluorescence was observed during laboratory Raman analyses. However, this fluorescence decreased with laser exposure over time and peaks were observed at 416, 495, 1008, and 1137 cm^{-1} , which correspond to gypsum (Figure 8).

4.3. Raman Spectra of Bacterial Mats and Clamshells

[26] Work by Pasteris et al. [2001] showed that bacterially produced elemental sulfur in an S_8 ring configuration (major peaks at ~ 220 and 474 cm^{-1}) could be detected in bacterial mats by Raman spectroscopy in the laboratory. Their work used a laser Raman microprobe to focus the laser spot (on the order of microns) on vesicles in *Thioploca* and *Beggiatoa* collected from cold seep sites in Monterey Bay. Due to its strong Raman scattering efficiency, bacterial sulfur should be

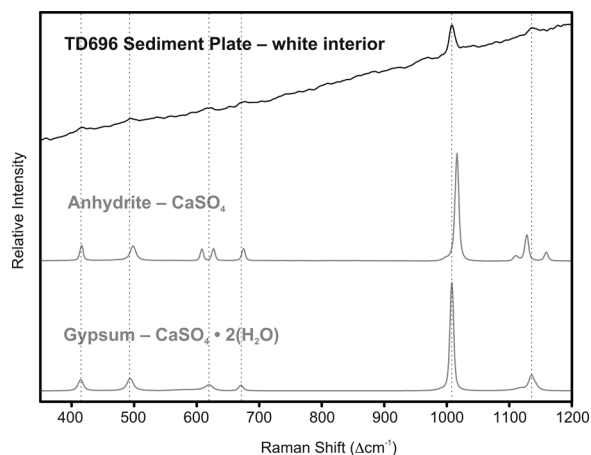


Figure 8. Raman spectrum obtained in the lab of a Sea Cliff rock compared to spectra of anhydrite and gypsum. The primary bands observed in the spectrum correspond well to gypsum (dashed lines).

detectable in situ on the seafloor using optics with larger spot sizes (on the order of tens of microns).

[27] In situ spectra of bacterial mats were collected in the Sea Cliff Hydrothermal Field and at Hydrate Ridge. At Sea Cliff, no large beds of bacterial mat were observed on the seafloor. Blue ciliate mats were present between the ridges of active venting. However, no identifiable Raman peaks (sulfur or otherwise) were observed from this material. Spectra collected from the blue mats showed the seawater in the optical path (peaks from water and sulfate), and broad fluorescence peaks in the 600–700 nm region.

[28] Some white bacterial mats were present on active chimneys in the Sea Cliff field, but they were difficult to visually discriminate from the white anhydrite of the chimney. While attempting to collect spectra of the chimney material at the orifice, spectra of bacterial mat were obtained serendipitously. The spectra contain the characteristic sulfur bands at ~ 220 and 474 cm^{-1} (Figure 9). No bands from anhydrite were observed. However, very weak bands at ~ 202 and 464 cm^{-1} may indicate the presence of quartz. Although quartz is the thermodynamically stable phase that should form from high-temperature vent fluids, amorphous silica is more typically observed [Von Damm et al., 2006]. Amorphous silica has a very broad ($\sim 100 \text{ cm}^{-1}$) Raman band at $\sim 470 \text{ cm}^{-1}$ [Kailer et al., 1999]. No quartz has been observed in samples collected from the Sea Cliff Hydrothermal Field (R. A. Zierenberg, personal communication, 2006).

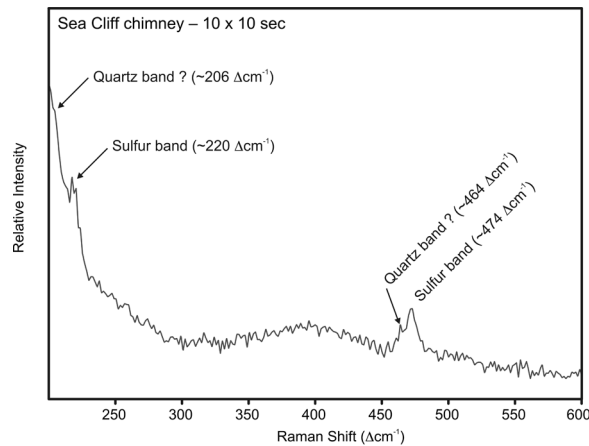


Figure 9. Raman spectrum of bacterial sulfur obtained while trying to analyze the orifice of an active chimney. Sulfur bands are observed at ~ 220 and $\sim 474 \text{ Δcm}^{-1}$. Although no anhydrite bands were observed, a weak quartz signature (bands at ~ 206 and $\sim 464 \text{ Δcm}^{-1}$) is detected.

[29] Large bacterial mats were observed on the seafloor at Hydrate Ridge. DORISS was deployed to look at red mats on NHR and white mats on SHR. In both cases, PUP was off-loaded onto the seafloor and used to position the DORISS optical head (using the noncontact optic) over the mats. As with the data from Sea Cliff, some spectra showed broad fluorescence bands in the 600–700 nm region. The four spectra collected at the red mat (10 accumulations \times 10 sec exposures) show the 474 Δcm^{-1} band which suggests the presence of elemental sulfur.

[30] Raman spectra were collected at the white mat on SHR (Figure 10). These spectra contain the primary sulfur bands at ~ 218 , 437 , and 474 Δcm^{-1} . These spectra also show bands at ~ 1159 and 1524 Δcm^{-1} which may be due to the presence of beta-carotene. Green lasers are known to generate resonance Raman scattering from carotenoids, and beta-carotene has been thus detected in Raman analyses of corals, shells, and lichens [Holder et al., 2000; Kaczorowska et al., 2003; Urmos et al., 1991; Withnall et al., 2003]. Spectra were also obtained at 1 mm increments in a 10 mm transect across the mat on SHR (Figure 11). Of the ten spectra, five indicated the presence of sulfur, four showed no sulfur bands, and one was saturated with fluorescence. The nonsulfur spectra contained bands from seawater (i.e., sulfate and water bands) and beta-carotene. In one case, the 1086 Δcm^{-1} calcium carbonate band was observed, most

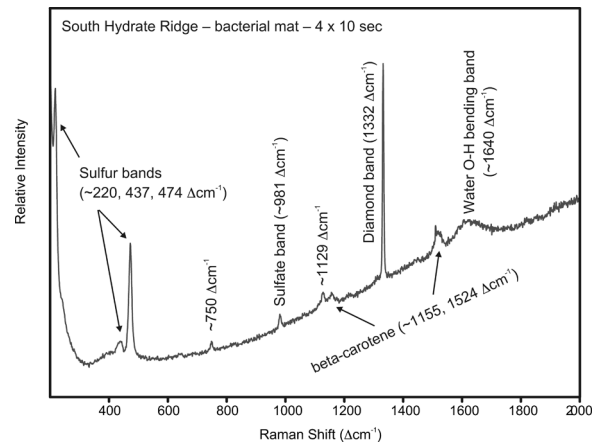


Figure 10. Raman spectrum of a bacterial mat at South Hydrate Ridge. Strong sulfur bands are observed at ~ 220 , 473 , and 474 Δcm^{-1} . Water and sulfate bands are present because seawater is in the optical path. The diamond band (1332 Δcm^{-1}) provides a calibration reference. Bands characteristic of beta carotene are observed at ~ 1155 and $\sim 1524 \text{ Δcm}^{-1}$.

likely due to the carbonate crusts in the area or from shells that were visible amid the bacterial mat. In this instance, the weaker Raman bands, which allow one to discriminate between calcite and aragonite were not detected. Aragonite and calcite are polymorphs of calcium carbonate

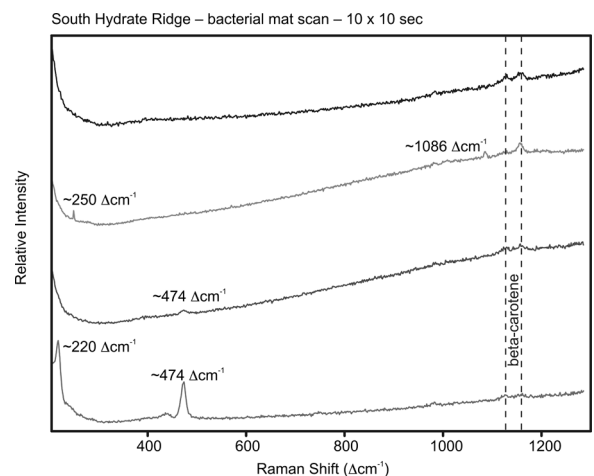


Figure 11. Raman spectra collected at 1 mm increments during a scan of a bacterial mat at South Hydrate Ridge. The top two spectra have no sulfur bands. The second from the top shows a weak 1086 Δcm^{-1} band which is characteristic of calcium carbonate. The bottom two spectra show sulfur bands (~ 220 and 474 Δcm^{-1}). All spectra show ~ 1159 and $\sim 1524 \text{ Δcm}^{-1}$ bands which are characteristic of beta-carotene.

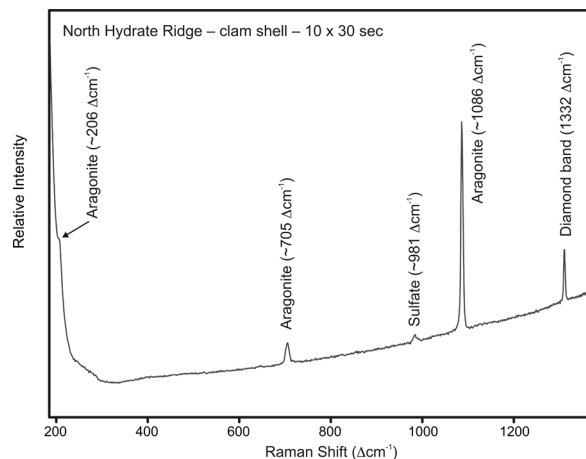


Figure 12. Raman spectrum of a clamshell on the seafloor at Hydrate Ridge. The $1086 \Delta\text{cm}^{-1}$ band is characteristic of calcium carbonate. The 206 and $705 \Delta\text{cm}^{-1}$ bands indicate that the calcium carbonate is aragonite rather than calcite (both are CaCO_3). The diamond band ($1332 \Delta\text{cm}^{-1}$) provides a calibration reference. The sulfate band is present because seawater is in the optical path.

(CaCO_3) which can be distinguished from one another by their minor Raman bands: aragonite, ~ 206 and $\sim 705 \Delta\text{cm}^{-1}$; calcite, ~ 281 and $\sim 711 \Delta\text{cm}^{-1}$ [Urmos *et al.*, 1991]. However, on a subsequent dive to SHR, spectra were acquired from a clamshell on the seafloor (Figure 12). The spectra contained the primary carbonate band at $\sim 1086 \Delta\text{cm}^{-1}$, and minor bands at ~ 206 and $\sim 705 \Delta\text{cm}^{-1}$, which indicate the presence of aragonite. In previous Raman work we have observed the presence of both calcite and aragonite in seafloor shells [White *et al.*, 2005], thus extending the work of Urmos *et al.* [1991] to in situ conditions.

5. Future Improvements

5.1. Instrumentation Advancements

[31] In the case of volatiles dissolved in hydrothermal fluids, the instrument sensitivity must be improved to enable the detection of these species at low concentrations. Increased laser power at the target, improved optical throughput, and CCD cameras with higher quantum efficiencies can help to improve sensitivity. Increasing the sample volume through new sampling optics can also help to improve sensitivity particularly for transparent and semi-transparent targets. Experiments have been

conducted with a new large-volume optical probe from KOSI attempting to directly measure the seawater carbonate system [Brewer *et al.*, 2004b].

[32] When analyzing high-temperature hydrothermal fluids, a noncontact optic must be used due to the precipitation of sulfide coating onto an immersion-type optic. If low-temperature venting is to be analyzed, an immersion type optic can be used. To increase sensitivity, a large volume optic or a long-path length liquid core optical fiber can be used. In either case, if a Raman instrument is to be deployed long-term in a vent field (i.e., as a part of a seafloor observatory), methods will have to be implemented to keep the optics free from biological or mineralogical fouling.

[33] Fluorescence can overwhelm Raman signals in some cases. Methods to deal with fluorescence include time resolved Raman spectroscopy and the use of longer wavelength excitation lasers [Ferraro *et al.*, 2003]. The Raman effect occurs on time-scales of picoseconds. Fluorescence, which can be orders of magnitude more intense than the Raman signal occurs on timescales of nanoseconds. Thus picosecond time gating of the laser and the spectrometer can be used to discriminate the Raman signal from the fluorescence [e.g., Matousek *et al.*, 1999]. Industrial applications often use a 785 nm laser, which does not induce as much fluorescence as a 532 nm laser. However, the intensity of the Raman scattered signal decreases with increasing wavelength. Therefore reduction of fluorescence must be weighed against the resulting reduction in signal. In some cases fluorescence will decrease over time with continued exposure to the excitation beam. Thus simply waiting for 5–10 minutes can result in spectra with less fluorescence and identifiable peaks. Additionally, decreasing the laser power can reduce fluorescence to the point that longer exposure times can be used to detect mineral peaks. Both of these effects were observed during laboratory analyses.

5.2. Operational/Processing Advancements

[34] The use of a noncontact optic increases complexity in the data as ambient seawater in the optical path will produce a small contribution to the acquired spectrum. Weak O-H stretching bands from seawater in the unfocused portion of the optical path will be superimposed onto the stronger O-H stretching bands of the high-temperature fluid in the focal volume. Therefore advanced data processing techniques will be required to remove the ambient seawater component, particularly if the



data will be used to obtain vent fluid temperature. Laboratory work is needed to better characterize the Raman spectrum of water at the pressures, temperatures, and fluid compositions (both ionic composition and strength) found at hydrothermal vents.

[35] Due to the heterogeneous nature of targets such as rocks and bacterial mats, a better method of visually locating the laser spot is required. A through-the-lens visualization system would be ideal, however to implement this requires the addition of a movable mirror (introducing a possible failure point) or a beam splitter (which would reduce optical throughput). Additionally, although Raman spectroscopy does not require sample preparation, in some cases it may be necessary to split rock samples in situ to allow analysis of the sample interior.

6. Conclusions

[36] Raman spectroscopy is rapidly being developed into a useful expeditionary tool with much potential for use in hydrothermal vent environments. Data were collected from high-temperature vent fluids, minerals, and bacterial mats. The DORISS system was capable of identifying mineral targets such as barite, anhydrite, and calcium carbonate, and detecting high-temperature water; however, the present system did not have the sensitivity to detect the Raman signal of the dissolved gases in the vent fluid. In order to improve the usefulness of the instrument and to advance laser Raman spectroscopy as a deep-sea in situ technique, a number of advancements in instrumentation (including size, weight, stability and sensitivity), operations, and postprocessing must be made. Some of these advancements will be present in the second generation DORISS instrument (DORISS II) scheduled to be deployed by MBARI in late-2005.

Acknowledgments

[37] We thank the captain and crew of the R/V *Western Flyer* and the pilots of the ROV *Tiburón*. This project benefited greatly from the engineering expertise of Alana Sherman, Mark Brown, and John Ferreira. Funding was provided by the David & Lucile Packard Foundation.

References

Abe, N., and M. Ito (1978), Effects of hydrogen bonding on the Raman intensities of methanol, ethanol and water, *J. Raman Spectrosc.*, **7**, 161–167.

- Baker, E. T., G. J. Massoth, R. Collier, J. H. Trefry, D. Kadko, T. A. Nelsen, P. A. Rona, and J. Lupton (1987), Evidence for high-temperature hydrothermal venting on the Gorda Ridge, northeast Pacific Ocean, *Deep Sea Res., Part A*, **34**, 1461–1476.
- Battaglia, T. M., E. E. Dunn, M. D. Lilley, J. Holloway, B. K. Dable, B. J. Marquardt, and K. S. Booksh (2004), Development of an in situ fiber optic Raman system to monitor hydrothermal vents, *Analyst*, **129**, 602–606.
- Becucci, M., S. Cavalieri, R. Eramo, L. Fini, and M. Materazzi (1999), Accuracy of remote sensing of water temperature by Raman spectroscopy, *Appl. Opt.*, **38**, 928–931.
- Boetius, A., K. Ravensschlag, C. J. Schubert, D. Rickert, R. Widdel, A. Gleseke, R. Amann, B. B. Jorgensen, U. Witte, and O. Pfannkuche (2000), A marine microbial consortium apparently mediating anaerobic oxidation of methane, *Nature*, **407**, 623–626.
- Bohrmann, G., J. Greinert, E. Suess, and M. E. Torres (1998), Authigenic carbonates from the Cascadia subduction zone and their relation to gas hydrate stability, *Geology*, **26**, 647–650.
- Brewer, P. G., G. E. Malby, J. D. Pasteris, S. N. White, E. T. Peltzer, B. Wopenka, J. Freeman, and M. O. Brown (2004a), Development of a laser Raman spectrometer for deep-ocean science, *Deep Sea Res., Part I*, **51**, doi:10.1016/j.dsr.2003.1011.1005.
- Brewer, P. G., R. M. Dunk, S. N. White, E. T. Peltzer, B. Bowie, and P. M. Walz (2004b), First attempts at direct Raman detection of the oceanic carbonate system, *Eos Trans. AGU*, **85**(47), Fall Meet. Suppl., Abstract OS43B-557.
- Brill, T. B. (2000), Geothermal vents and chemical processing: The infrared spectroscopy of hydrothermal reactions, *J. Phys. Chem. A*, **104**, 4343–4351.
- Busing, W. R., and D. F. Hornig (1961), The effect of dissolved KBr, KOH, or HCl on the Raman spectrum of water, *J. Phys. Chem.*, **65**, 284–292.
- Ferraro, J. R., K. Nakamoto, and C. W. Brown (2003), *Introductory Raman Spectroscopy*, 2nd ed., Elsevier, New York.
- Frantz, J. D. (1998), Raman spectra of potassium carbonate and bicarbonate aqueous fluids at elevated temperatures and pressures: Comparison with theoretical simulations, *Chem. Geol.*, **152**, 211–225.
- Frantz, J. D. (2000), Salts of aliphatic carboxylic acids: Raman spectra and ion pairing in hydrothermal solutions containing sodium and calcium acetates, *Chem. Geol.*, **164**, 1–20.
- Frantz, J. D., J. Dubessy, and B. Mysen (1993), An optical cell for Raman spectroscopic studies of supercritical fluids and its application to the study of water to 500°C and 2000 bar, *Chem. Geol.*, **106**, 9–26.
- Haskin, L. A., A. Wang, K. M. Rockow, B. L. Jolliff, R. L. Korotev, and K. M. Viskupic (1997), Raman spectroscopy for mineral identification and quantification for in situ planetary surface analysis: A point count method, *J. Geophys. Res.*, **102**, 19,293–19,306.
- Haymon, R. M., and M. Kastner (1981), Hot spring deposits on the East Pacific Rise at 21°N: Preliminary description of mineralogy and genesis, *Earth Planet. Sci. Lett.*, **53**, 363–381.
- Hester, K. C., S. N. White, E. T. Peltzer, P. G. Brewer, and E. D. Sloan (2006), Raman spectroscopic measurements of synthetic gas hydrates in the ocean, *Mar. Chem.*, **98**, 304–314.
- Holder, J. M., D. D. Wynn-Williams, F. Rull Perez, and H. G. M. Edwards (2000), Raman spectroscopy of pigments and



- oxalates in situ within epilithic lichens: Acarospora from the Antarctic and Mediterranean, *New Phytol.*, *145*, 271–280.
- Kaczorowska, B., A. Hacura, T. Kupka, R. Wrzalik, E. Talik, G. Pasterny, and A. Matuszewska (2003), Spectroscopic characterization of natural corals, *Anal. Bioanal. Chem.*, *377*, 1032–1037.
- Kailer, A., K. G. Nickel, and Y. G. Gogotsi (1999), Raman microspectroscopy of nanocrystalline and amorphous phases in hardness indentations, *J. Raman Spectrosc.*, *30*, 939–946.
- Kawamoto, T., S. Ochiai, and H. Kagi (2004), Changes in the structure of water deduced from the pressure dependence of the Raman OH frequency, *J. Chem. Phys.*, *120*, 5867–5870.
- Matousek, P., M. Towrie, A. Stanley, and A. W. Parker (1999), Efficient rejection of fluorescence from Raman spectra using picosecond Kerr gating, *Appl. Spectrosc.*, *53*, 1485–1489.
- McGuire, M. M., K. J. Edwards, J. F. Banfield, and R. Hamers (2001), Kinetics, surface chemistry, and structural evolution of microbially mediated sulfide mineral dissolution, *Geochim. Cosmochim. Acta*, *65*, 1243–1258.
- Pasteris, J. D., J. J. Freeman, S. K. Goffredi, and K. R. Buck (2001), Raman spectroscopic and laser scanning confocal microscopic analysis of sulfur in living sulfur-precipitating marine bacteria, *Chem. Geol.*, *180*, 3–18.
- Pasteris, J. D., B. Wopenka, J. J. Freeman, P. G. Brewer, S. N. White, E. T. Peltzer, and G. E. Malby (2004), Raman spectroscopy in the deep ocean: Successes and challenges, *Appl. Spectrosc.*, *58*, 195A–208A.
- Ratcliffe, C. I., and D. E. Irish (1982), Vibrational spectral studies of solutions at elevated temperatures and pressures. 5. Raman studies of liquid water up to 300°C, *J. Phys. Chem.*, *86*, 4897–4905.
- Riddihough, R. P. (1980), Gorda plate motions from magnetic anomaly analysis, *Earth Planet. Sci. Lett.*, *51*, 163–170.
- Rochette, E. A., B. Bostick, G. Li, and S. Fendorf (2000), Kinetics of arsenate reduction by dissolved sulfide, *Environ. Sci. Technol.*, *34*, 4714–4720.
- Rona, P. A., and D. A. Clague (1989), Geologic controls of hydrothermal discharge on the northern Gorda Ridge, *Geology*, *17*, 1097–1101.
- Rona, P. A., R. P. Denlinger, M. R. Fisk, K. J. Howard, G. L. Taghon, K. D. Klitgord, J. S. McClain, G. R. McMurray, and J. C. Wiltshire (1990), Major off-axis hydrothermal activity on the northern Gorda Ridge, *Geology*, *18*, 493–496.
- Schoppelrei, J. W., M. L. Kieke, and T. B. Brill (1996), Spectroscopy of hydrothermal reactions. 2. Reactions and kinetic parameters of $[\text{NH}_3\text{OH}]\text{NO}_3$ and equilibria of $(\text{NH}_4)_2\text{CO}_3$ determined with a flow cell and FT Raman spectroscopy, *J. Phys. Chem.*, *100*, 7463–7470.
- Suess, E., et al. (1999), Gas hydrate destabilization: Enhanced dewatering, benthic material turnover and large methane plumes at the Cascadia convergent margin, *Earth Planet. Sci. Lett.*, *170*, 1–15.
- Terpstra, P., C. Combes, and A. Zwick (1990), Effect of salts on dynamics of water: A Raman spectroscopy study, *J. Chem. Phys.*, *92*, 65–70.
- Tivey, M. K. (1995), Modeling chimney growth and associated fluid flow at seafloor hydrothermal vent sites, in *Seafloor Hydrothermal Systems: Physical, Chemical, Biological, and Geological Interactions*, *Geophys. Monogr. Ser.*, vol. 91, edited by S. E. Humphris et al., AGU, Washington, D. C.
- Torres, M. E., J. McManus, D. E. Hammond, M. A. de Angelis, K. U. Heeschen, S. L. Colbert, M. D. Tryon, K. M. Brown, and E. Suess (2002), Fluid and chemical fluxes in and out of sediments hosting methane hydrate deposits on Hydrate Ridge, OR, I: Hydrological provinces, *Earth Planet. Sci. Lett.*, *201*, 252–540.
- Tryon, M. D., K. M. Brown, and M. E. Torres (2002), Fluid and chemical flux in and out of sediments hosting methane hydrate deposits on Hydrate Ridge, OR, II: Hydrological processes, *Earth Planet. Sci. Lett.*, *201*, 541–557.
- Urmos, J., S. K. Sharma, and F. T. Mackenzie (1991), Characterization of some biogenic carbonates with Raman spectroscopy, *Am. Mineral.*, *76*, 641–646.
- Von Damm, K. L., C. M. Parker, M. D. Lilley, D. A. Clague, R. A. Zierenberg, E. J. Olson, and J. S. McClain (2006), Chemistry of vent fluids and its implications for subsurface conditions at Sea Cliff hydrothermal field, Gorda Ridge, *Geochem. Geophys. Geosyst.*, *7*, Q05005, doi:10.1029/2005GC001034.
- Walrafen, G. E. (1964), Raman spectral studies of water structure, *J. Chem. Phys.*, *40*, 3249–3256.
- Wang, A., L. A. Haskin, and E. Cortez (1998), Prototype Raman spectroscopic sensor for in situ mineral characterization on planetary surfaces, *Appl. Spectrosc.*, *52*, 477–487.
- Wang, A., L. A. Haskin, A. L. Lane, T. J. Wdowiak, S. W. Squyres, R. J. Wilson, L. E. Hovland, K. S. Manatt, N. Raouf, and C. D. Smith (2003), Development of the Mars microbeam Raman spectrometer (MMRS), *J. Geophys. Res.*, *108*(E1), 5005, doi:10.1029/2002JE001902.
- White, S. N., W. J. Kirkwood, A. D. Sherman, M. O. Brown, R. Henthorn, K. A. Salamy, P. M. Walz, E. T. Peltzer, and P. G. Brewer (2005), Development and deployment of a precision underwater positioning system for in situ laser Raman spectroscopy in the deep ocean, *Deep Sea Res., Part I*, *52*, 2376–2389.
- White, S. N., P. G. Brewer, and E. T. Peltzer (2006), Determination of gas bubble fractionation rates in the deep ocean by laser Raman spectroscopy, *Mar. Chem.*, *99*, 12–23.
- Withnall, R., B. Z. Chowdhry, J. Silver, H. G. M. Edwards, and L. F. C. de Olivera (2003), Raman spectra of carotenoids in natural products, *Spectrochim. Acta A*, *59*, 2207–2212.